Pressure-induced structural phase transitions and phonon anomalies in ReO_3: Raman and first-principles study

D. V. S. Muthu,[1] Pallavi Teredesai,[1,2] S. Saha,[1,3] Suchitra ,[4] U. V. Waghmare,[4] A. K. Sood,[1,5] and C. N. R. Rao[5]

[1]*Department of Physics, Indian Institute of Science, Bangalore 560012, India*

[2]*Navrachana University, Vadodara 391410, India*

[3]*Department of Physics, National University of Singapore, Singapore 117411*

[4]*Theoretical Science Unit, Jawaharlal Nehru Center for Advanced Scientific Research, Jakkur P.O., Bangalore 560064, India*

[5]*Chemistry and Physics of Materials Unit, New Chemistry Unit and International Centre for Materials Science, Jawaharlal Nehru Centre for Advanced Scientific Research, Jakkur P.O., Bangalore 560064, India*

(Received 17 February 2015; revised manuscript received 28 April 2015; published 19 June 2015)

We report high-pressure Raman-scattering studies on single-crystal ReO_3 up to 26.9 GPa at room temperature, complemented by first-principles density functional calculations to assign the modes and to develop understanding of the subtle features of the low-pressure phase transition. The pressure (P) dependence of phonon frequencies (ω) reveals three phase transitions at 0.6, 3, and 12.5 GPa with characteristic splitting and changes in the slope of $\omega(P)$. Our first-principles theoretical analysis confirms the role of the rotational modes of ReO_6, M_3, to the lowest pressure structural transition, and shows that the transition from the $Pm3m$ to the $Im3$ structure is a weak first-order transition, originating from the strong anharmonic coupling of the M_3 modes with the acoustic modes (strain).

DOI: 10.1103/PhysRevB.91.224308 PACS number(s): 78.30.−j, 63.20.dk, 64.60.−i

I. INTRODUCTION

ABO_3 perovskite oxides exhibit a diverse range of phenomena ranging from magnetoresistance, superconductivity to ferroelectricity [1]. Typically, the insulating perovskite oxides, such as $BaTiO_3$, are known to commonly exhibit temperature- (T-) induced structural phase transitions in which the vanishing occupation of d orbitals of a transition-metal ion at the B site is a key to its off-centering as well as to the symmetry lowering structural instability. In contrast, T-dependent structural transitions are not common in metallic perovskite oxides, which typically have the d orbitals of their transition metal partially occupied by electrons. Competing structural instabilities in a perovskite involve rotations of the BO_6 octahedra, which are not excluded by the partial occupancy of d orbitals of the B cation [2]. When the size of the B cation relative to that of the A cation is large, the cubic perovskite structure can be unstable with respect to such octahedral rotational modes, and this can be another factor that can lead to structural transitions [1] and be used to understand fundamentally interesting structural transitions in metallic perovskite oxides. From this angle, ReO_3 is a rather interesting metallic perovskite oxide having conductivity within a factor of 6 of that of copper at room temperature and ∼100% reflectivity below the plasma edge at 2.1 eV. Here, the A cation is completely missing, and four pressure-dependent (but interestingly no temperature-dependent) structural transitions are observed.

At ambient pressure, the structure of ReO_3 is cubic (space group $Pm3m$) consisting of corner-linked ReO_6 octahedra and linear Re-O-Re bonds. The empty A cation site in ReO_3 promotes structural instabilities involving rotations of the rigid ReO_6 octahedra. The early interest in ReO_3 was triggered by an observation of a supposedly continuous phase transition at ∼0.5 GPa at room temperature with the compressibility being an order of magnitude higher in the high-pressure phase [3] (and hence termed as "compressibility collapse transition"). Early neutron-diffraction measurements showed that the high-pressure phase is tetragonal ($P4/mbm$), which transforms at a slightly higher pressure of 0.72 GPa to the cubic II ($Im3$) phase [4]. However, recent neutron-diffraction studies do not find any evidence of the tetragonal ($P4/mbm$) intermediate phase between the two cubic structures [5]. The softening of the M_3 phonon mode was suggested to be the driving force behind the $Pm3m$ to $Im3$ pressure transition. X-ray diffraction at high pressures by Jorgensen *et al.* [6] showed three other phase transitions; a cubic II ($Im3$) phase to a monoclinic MnF_3 related phase at 3 GPa to the rhombohedral VF_3 related phase (rhombohedral I) at 12 GPa and to another rhombohedral phase (rhombohedral II) at 38 GPa. Subsequent high-pressure x-ray diffraction studies by Suzuki *et al.* [7] did not observe the monoclinic phase and showed that the cubic phase and rhombohedral I phase coexist in the pressure range of 8–18 GPa. Biswas *et al.* [8] have recently reported pressure-induced phase transitions in nanocrystalline ReO_3 using synchrotron x-ray diffraction. They have shown that the ambient pressure cubic I phase ($Pm3m$) changes to the monoclinic phase ($C2/c$) at ∼0.3 GPa and from the monoclinic to a rhombohedral I phase ($R3c$) at ∼6.7 GPa and finally to a rhombohedral II phase at ∼20.3 GPa.

Purans *et al.* [9] have carried out Raman measurements at room temperature and ambient pressure. We carry out a high-pressure Raman study of crystalline ReO_3 here. We have carried out high-pressure Raman measurements up to 26.9 GPa on single crystals of ReO_3 showing three phase transitions at 0.6, 3, and 12.5 GPa. The pressure derivatives of the phonon frequencies have been determined. Our results for the high-pressure transitions corroborate the x-ray diffraction results of Jorgensen *et al.* [4]. However, the low-pressure structural transition at $P \sim 0.6$ GPa is quite intriguing, and we

*Corresponding author: asood@physics.iisc.ernet.in

use first-principles density functional theory (DFT) to develop an understanding of the same.

First-principles calculations of electronic structure have been useful in the analysis of electronic properties of ReO_3 revealing that it is a normal Fermi-liquid-type metal [10]. DFT-based calculations also help to understand the relation between the electronic and the structural properties of ReO_3 and related oxides [11]. Recently, lattice dynamics and negative thermal expansion exhibited by ReO_3 at low temperature have been modeled by treating results of the DFT calculations within a quasiharmonic approximation [12]. Although the zone-center phonon frequencies determined in Refs. [11,12] confirmed the stability of ReO_3 with respect to uniform structural distortions in contrast to that of WO_3, the large discrepancy between the calculated and experimental frequencies is quite striking.

We have employed various flavors and methods of DFT calculations to sort this out and discuss the possible reasons for the discrepancy in terms of electron-phonon coupling and anharmonicity. We determine complete phonon dispersion and two-phonon density of states (DOS) to assign the observed Raman bands in the cubic phase. Finally, we focus on the low-pressure structural phase transition and corroborate experimental observations through determination of pressure-dependent phonon frequencies of the $Pm3m$ and $Im3$ phases. Our theoretical analysis suggests that the transition between these two phases is a weakly first-order (and not the second-order) transition and highlights the *marginal* thermal stability of the cubic structure of ReO_3.

In Sec. II, we describe the details of our experimental work and computational methods and present our results along with the discussion in Sec. III and conclude in Sec. IV.

II. METHODS

Experiment

ReO_3 single crystals were prepared by the vapor transport method [13]. Raman spectroscopic measurements were carried out at room temperature using 514.5-nm excitation from an argon-ion laser and a triple monochromator DILOR XY Raman spectrometer equipped with a liquid-nitrogen-cooled CCD. Pressure was generated using a diamond-anvil cell, using 16:3:1 methanol:ethanol:water as a pressure transmitting medium, and a ruby fluorescence method [14] was used for pressure calibration.

Our first-principles calculations are based on QUANTUM ESPRESSO [15] implementation of the DFT at different levels of approximations to the functional description of the exchange-correlation energy: local density approximation (LDA), generalized gradient corrected approximation (GGA), and LDA with an on-site correlation term with a Hubbard U parameter (LDA + U). We have used ultrasoft [16] as well as optimized norm-conserving (NC) pseudopotentials [17] to represent the interaction between the ions and the valence electrons. Nonlinear core corrections were included to capture the effects of the exchange-correlation interaction between valence and core electrons. To validate the results obtained from our calculations based on pseudopotentials, we determined the structure and zone-center phonon frequencies using the frozen phonon method with all electron calculations with WIEN2K [18] interfaced with the PHONOPY program [19]. For the *Im3* phase of ReO_3, the crystal structure was determined through minimization of total energy using Hellmann-Feynman forces on atoms within the Broyden-Fletcher-Goldfarb-Shanno algorithm. Vibrational frequencies and related dynamical properties were determined using the pseudopotential framework of the density functional perturbation theory as implemented in QUANTUM ESPRESSO [15].

III. RESULTS AND DISCUSSIONS

A. Raman spectrum at ambient conditions

At ambient conditions, ReO_3 crystallizes in the $Pm3m$ space group with the Bravais unit cell containing 1 formula unit (f.u.) of ReO_3. The optical phonons belong to irreducible representation $2F_{1u}+F_{2u}$. The $F_{1u}(\Gamma_{15})$ modes are infrared-(IR-) active involving displacements of Re and oxygen atoms with frequencies of 905 and 315 cm^{-1} [20]. The $F_{2u}(\Gamma_{25})$ mode is both infrared and Raman silent and involves only oxygen displacements. Figure 1 (lowest panel) shows the Raman spectrum of ReO_3 at ambient pressure, which agrees well with the spectrum published by Ishii *et al.* [20]. Since there is no Raman-active zone-center mode, the observed Raman bands at 259, 350, 418, 516, 600, 677, 768, 891, 944, 1026, and

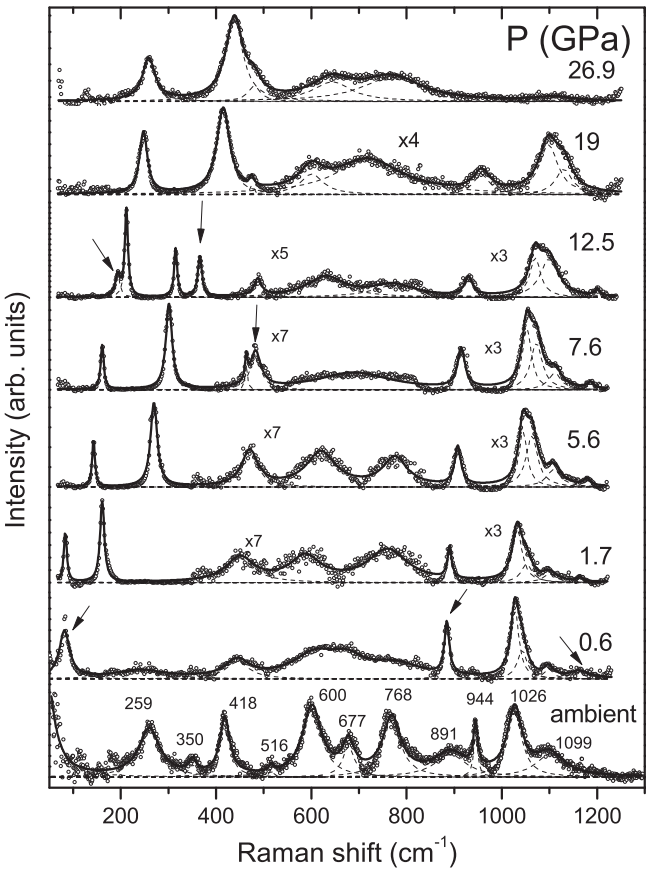

FIG. 1. Raman spectra recorded at ambient and various high pressures: in the region of 50–1300 cm^{-1}. The solid lines are fit to a sum of Lorentzians to the data shown by open circles. The arrows indicate the appearance of new modes owing to pressure-induced phase transitions.

1099 cm^{-1} are due to second-order Raman scattering involving different combinations. We will assign these Raman bands later based on the two-phonon density of states determined by first-principles DFT calculations.

B. Pressure-induced phase transitions

Figure 1 shows Raman spectra of ReO_3 at various pressures where the solid lines represent fitted Lorentzian functions. The spectra clearly show changes in the Raman modes around 0.6, 3, and 12.5 GPa. The intensity of the Raman modes at various pressures in the region of 500–800 cm^{-1} is very weak, and the zoomed version of this region is shown in Fig. 1. Figure 2 shows the pressure dependence of the frequencies of the various Raman modes obtained from the Lorentzian fits to the data. The possible phase transitions under pressure are identified by slope changes in the pressure dependence of mode frequencies and the appearance or disappearance of Raman bands (as marked by arrows in Fig. 1). The transition pressures are marked at 0.6, 3, and 12.5 GPa with dotted lines. The mode frequencies are linearly fitted with pressure and the slope $d\omega/dp$ (in units of cm^{-1}/GPa) is written by the side of the lines in Fig. 2. The pressure dependence of mode frequencies in the 500–800-cm^{-1} region was difficult to follow because of the weak intensities. Table I lists the various mode frequencies and their pressure dependences. At 0.4 GPa, a new mode is seen at 62 cm^{-1}. At 0.6 GPa, this mode shifts to ~80 cm^{-1}, and new modes at 880 and 1180 cm^{-1} appear at this pressure (marked by arrows in Fig. 1). The intense mode at 944 cm^{-1} and the weak mode at 891 cm^{-1} disappear at this pressure. These changes can be attributed to the transition from the cubic I ($Pm3m$) to a cubic II ($Im3$) phase as reported by high-pressure x-ray diffraction [6]. Around 1 GPa another low-frequency mode near 65 cm^{-1} appears as can be clearly seen at 1.7 GPa. At 1.7 GPa, another new mode is seen as a shoulder close to 1026 cm^{-1}. There is a drastic change in the slope of the two low-frequency modes at about 3 GPa (Fig. 2). This can be associated with the phase transition from the cubic II ($Im3$) to a monoclinic ($C2/c$) phase observed in x-ray diffraction [6]. It is clearly seen from Fig. 1 that at 7.6 GP the mode at 418 cm^{-1} splits into a doublet with frequencies 464 and 481 cm^{-1}. At ~12.5 GPa, the two strong low-frequency modes near 180 and 300 cm^{-1} split into doublets (Fig. 1), accompanied by changes in the slope of the modes at this pressure (Fig. 2), and the mode at 1099 cm^{-1} disappears. These changes can be associated with the phase transition from the monoclinic ($C2/c$) to a rhombohedral I ($R3c$) phase seen earlier in x-ray studies [6]. The changes in Raman spectra at 7.6 GPa do not have any signatures in the reported x-ray data which show the sample may remain in the monoclinic phase. The two low-frequency modes persist until the highest pressure of 26.9 GPa in our study. On decompression from the highest pressure the sample recovered to the original phase.

TABLE I. Mode frequencies and the corresponding $d\omega/dp$ of different phases. The mode frequencies in column 1 refer to the values at 0.6 GPa, except when they are at slightly different pressures indicated in the column.

	$d\omega/dp$ (cm^{-1}/GPa)		
Mode frequency (cm^{-1})	Pressure range 0.6–3 GPa cubic II	Pressure range 3–12 GPa monoclinic	Pressure range above 12.5 GPa rhombohedral II
62 (at 0.4 GPa)	76	14.6	5.8
65 (at 1.0 GPa)	22	7.5	3.6
447	5.4	5.4 0.8	0.8
886	3.7	3.7	3.7
1033	3.3	3.3	3.3
1054 (at 1.7 GPa)	4.3	4.3	4.3
1094	2.5	2.5	
1164	3.2	3.2	3.2

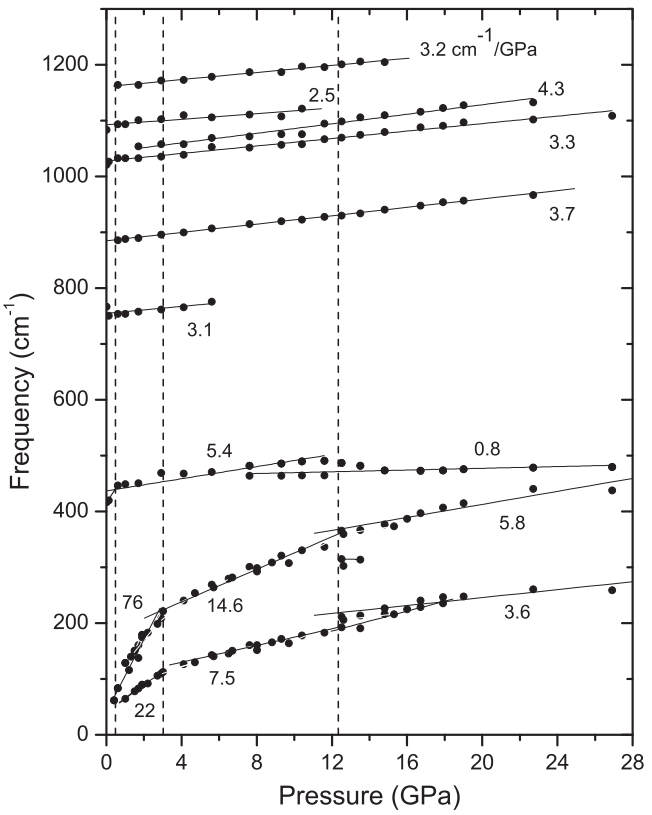

FIG. 2. Pressure dependence of the frequencies of various Raman modes. The vertical dashed lines represent the phase-transition pressures.

C. First-principles theoretical analysis

1. Zone-center phonons of the cubic structure

As mentioned before, the cubic $Pm3m$ structure of ReO_3 has $2F_{1u}(IR)+F_{2u}$ optical phonons at the Γ point. Our results for frequencies of the infrared-active phonons obtained with different exchange-correlation approximations and pseudopotentials are given in Table II. We note that: (a) Our results obtained with the NC pseudopotential-based DFT calculations are close to the experimental values but differ from those obtained with full potential linear muffin-tin orbital (LMTO) calculations [11], and (b) the change in pseudopotentials results in a relatively large change in the highest-frequency infrared-active mode.

TABLE II. Calculated zone-center phonons frequencies (in cm^{-1}) of the cubic ReO_3.

NC LDA	USPP LDA	USPP LDA + U = 1 eV	USPP GGA	WIEN2K LDA	Catlow LDA [9]	Experiment [16]
359	378	383	358 (IR)	373	215 (IR)	315 (IR)
393 (IR)	386 (IR)	384 (IR)	375	384 (IR)	433	
898 (IR)	759 (IR)	725 (IR)	702 (IR)	755 (IR)	760 (IR)	905 (IR)

The discrepancy between the experimental values [20] and our estimates of phonon frequencies as well as those from earlier calculations [11,12] is larger than the typical DFT results. Based on our results (Table II), use of different DFT functionals (LDA versus GGA) or inclusion of stronger correlations (LDA versus LDA + U) is unlikely to explain such a large difference. It is found that the highest-frequency mode is quite sensitive to the choice of (norm-conserving versus ultrasoft) pseudopotential (and demonstrated later that it is also very sensitive to pressure). In order to benchmark pseudopotential-based calculations, we have performed full potential calculations using WIEN2K within the LDA and obtained a theoretical lattice constant of 3.73 Å by fitting the Murnaghan equation of state to the energy versus volume curve. At this lattice constant, we determined the zone-center phonon frequencies of ReO_3 using atomic forces calculated with WIEN2K for configurations generated by displacing each of the atoms by 0.01 Å at a time and a frozen phonon method to obtain force constant matrix with a code PHONOPY. The phonon frequencies obtained using full potential and LDA ultrasoft pseudopotential (LDA USPP) calculations are in quite good agreement (Table II). Our estimates of the highest-frequency IR-active mode obtained using LDA USPP and WIEN2K LDA (Table II) are also close to those obtained with full potential LMTO calculations [11]. Although LDA with NC pseudopotential-based calculations seem to yield phonon properties closer to the experiment, it may be spurious because the pseudopotential-based calculations should ideally be consistent with all-electron calculations (e.g., WIEN2K) for the same flavor of exchange-correlation energy. As other properties are well explained within the LDA by USPP, we have carried out the rest of the calculations within the LDA using USPP at the theoretical lattice constant (a) of 3.72 Å, which is close to the experimental value of 3.75 Å.

2. *Phonon dispersion and the two-phonon density of states*

Using DFT linear response we have obtained dynamical matrices at Bloch wave vectors corresponding to high-symmetry points in the Brillouin zone (Γ, X, M, and R) and used Fourier interpolation to determine the dynamical matrices at an arbitrary Bloch vector. The phonon dispersion curves determined here from first principles are qualitatively similar to those computed empirically [20]. Our results for phonon dispersion (see Fig. 3) reveal that the softest optical modes are at the zone boundary: M, R, and X. The former two correspond to the rotational modes of the oxygen octahedra. The mode M_3 involves rotation of the ReO_6 octahedron around the z axis for $M = (110)\pi/a$ and is triply degenerate with M_3 modes at other M points [$(011)\pi/a$ and $(101)\pi/a$] that involve rotation around the x and y axes, respectively. The R_{25} mode is a triply degenerate mode involving rotations of ReO_6 around each of the Cartesian axes. When one of these modes is unstable (negative values of square of frequencies), the structure distorts through rotation of ReO_6 octahedra resulting in a cell-doubling structural transition. Mode X_5 is doubly degenerate and does not seem to be directly relevant to any of the observed transitions in ReO_3. Note that there is a gap in the phonon frequencies from 508 to 708 cm^{-1}. High-frequency phonons involve stretching of the Re-O bonds and are isolated from the rest. The modes at the R point (R_2 at 1037 cm^{-1} and R_{12} at 829 cm^{-1}) have the highest frequencies as they involve stretching and compression of Re-O bonds in alternate unit cells. These are significantly higher than in insulating perovskite oxides [2].

Lastly, the acoustic modes of ReO_3 are quite interesting: (a) the transverse acoustic (TA) phonons are much softer than the longitudinal acoustic (LA) phonons, implying that ReO_3 has a large bulk modulus but a rather low shear modulus, and (b) the branches of phonons containing rotational modes M_3 and R_{25} involve a strong mixing with branches of both LA and TA modes. Thus, we expect a strong dependence of M_3 and R_{25} modes on the isotropic and shear strains, and hence they should be quite relevant to pressure-induced structural phase transitions in ReO_3.

Since there is no Raman-active mode at the zone center, the bands observed in Fig. 1 are clearly second-order Raman modes. From the one-phonon and two-phonon density of states (Fig. 4), we attempt to assign overtones using the selection rules [20] (allowing for some errors as was evident in the Γ-point phonons) and information about various overtones available from the two-phonon DOS obtained by including only the overtones (Fig. 4): 259 cm^{-1}: 2 × M_3 at 99 cm^{-1}; 350 cm^{-1}: two phonons along the Σ line; 418 cm^{-1}: along the M to X or Σ lines; 600 cm^{-1}: 2 × X_1; 677 cm^{-1}: 2 × Γ_{25}

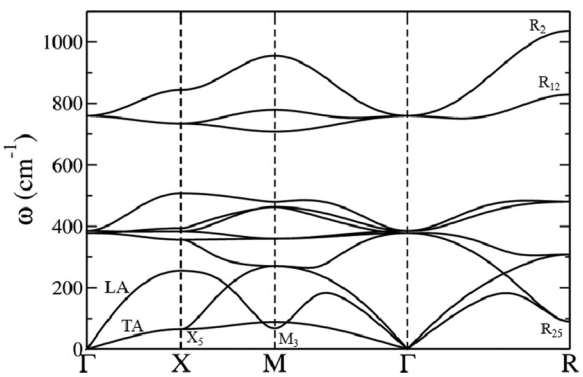

FIG. 3. Phonon dispersion of cubic ReO_3 determined from first principles.

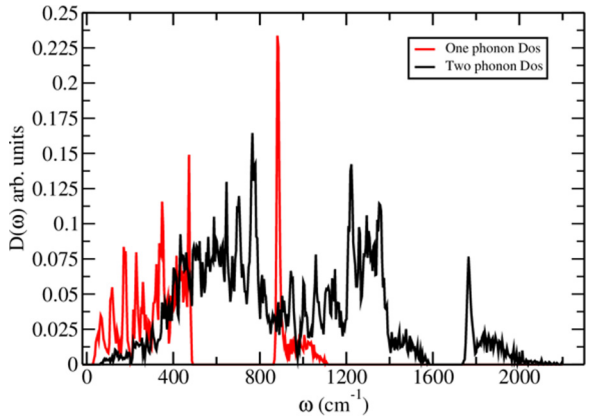

FIG. 4. (Color online) One- and two-phonon density of states of cubic ReO_3 (obtained using the LDA with the NC pseudopotential).

or $2 \times X_5$; 768 cm^{-1}: $2 \times X_5$; 1026 cm^{-1}: $2 \times X_1$ or $2 \times R_{15}$; 1085 cm^{-1}:$2 \times X_1$ or $2 \times R_{15}$.

3. *Pressure dependence of phonon frequencies*

To understand the observed pressure-dependent structural transitions in ReO_3, we first determine the pressure dependence of phonons at high-symmetry points in the Brillouin zone of the cubic ($Pm3m$) phase. At each wave vector, we find that the high-frequency phonons harden and lower-frequency phonons soften with pressure. At the Γ point (Fig. 5), only the highest energy Γ_{15} phonon is strongly dependent on pressure exhibiting an increase in frequency, and the rate of change of frequency with pressure is 6.2 cm^{-1}/GPa. This is similar to the pressure dependence of polar phonons in ferroelectric oxides [21]. In contrast, the lower-energy phonons of Γ_{25} symmetry exhibit gradual softening with pressure. The strong P dependence of the high-frequency Γ_{15} mode reflects its anharmonic coupling particularly with strain or the LA modes, which is very likely responsible for its T dependence and therefore may explain the discrepancy between its zero temperature calculated and observed frequencies (at room temperature).

The softest mode at the X point having X_5 symmetry softens further with pressure but remains stable. The M_3 and R_{25} phonons involving rotation of ReO_6 octahedra, which are the softest modes in the phonon spectrum of cubic ReO_3, soften further with a strong dependence on pressure similar to the one reported by Wdowik *et al.* [12]. Although most modes at the M point are weakly dependent on pressure (Fig. 5), the M_3 mode is found to exhibit the strongest and anomalous dependence on pressure and becomes unstable for an applied pressure of >3 GPa. This is the mode (along with its symmetry related modes at other M points) that is expected to be relevant to structural phase transition from cubic I to cubic II in ReO_3. Likewise, the R_{25} mode is found to be sensitive to pressure and becomes unstable at pressures above 5 GPa. Although M_3 is the first mode that becomes unstable as pressure is applied, our estimate of the pressure required for this instability to set in is significantly higher than the observed pressure at which the first structural transition occurs. As we will analyze later, this is because the transition is weakly first order and occurs through a third-order coupling with acoustic modes.

We have determined the pressure dependence of zone-center phonons of ReO_3 in the $Im3$ cubic II structure. The $Im3$ structure has a unit cell with 8 formula units, and Brillouin-zone folding gives the correspondence of its zone-center phonons with the phonons at Γ, X, M, and R points

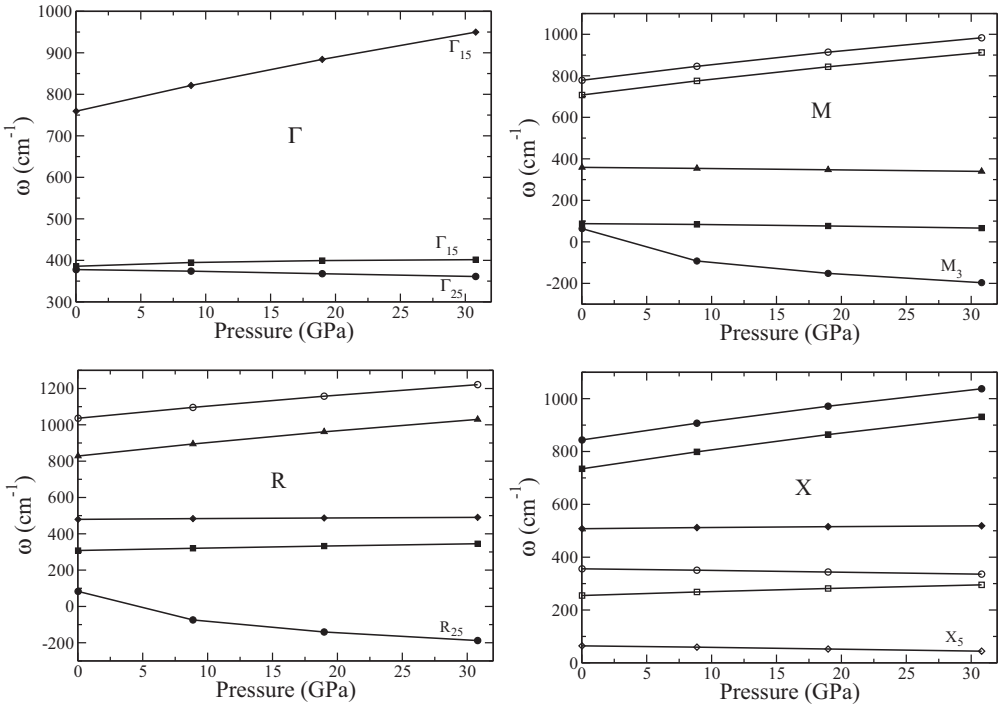

FIG. 5. Pressure dependence of frequencies of phonons at high-symmetry k points (Γ, X, M, and R) in the Brillouin zone of cubic ReO_3 using the LDA USPP.

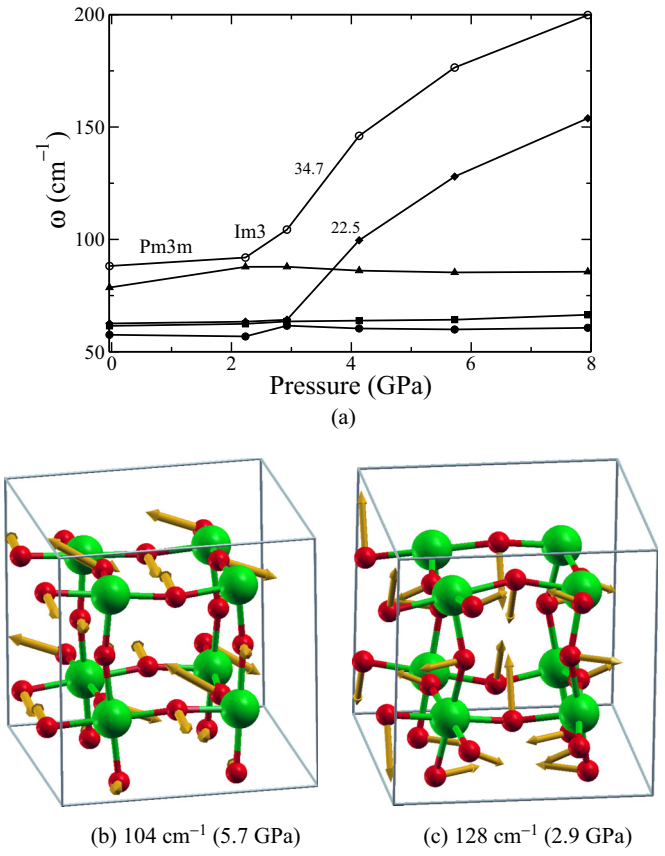

FIG. 6. (Color online) (a) Low-frequency phonons of ReO_3 as a function of pressure as it goes through a phase transition from the $Pm3m$ to the $Im3$ phase and atomic displacements at high and low pressures in (b) and (c), respectively. The large (green) spheres represent Re atoms whereas the O atoms are indicated by small (dark red) spheres.

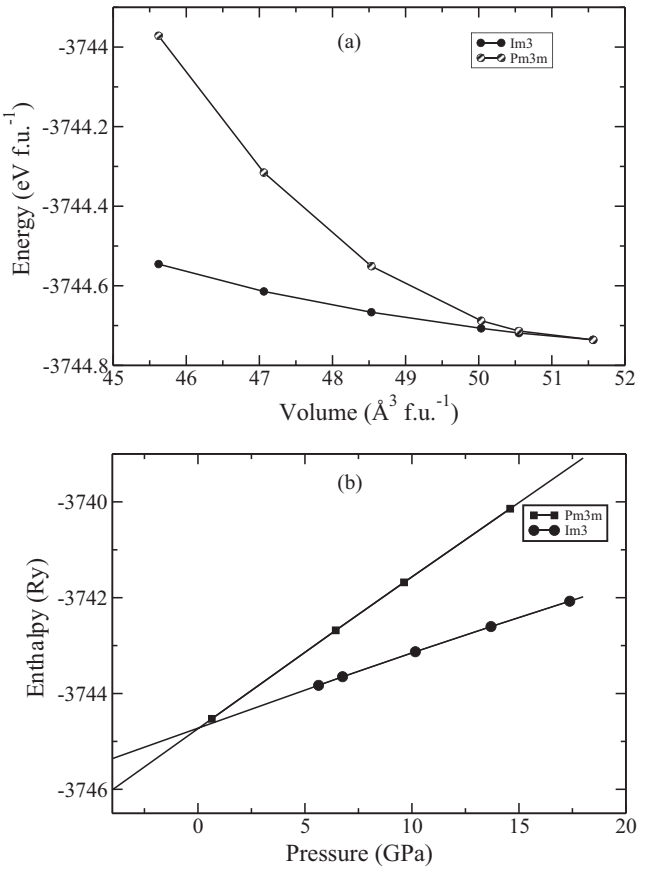

FIG. 7. (a) Total energy curve of the $Pm3m$ and the $Im3$ phases of ReO_3 and (b) their enthalpy change with pressure, calculated using pseudopotentials with the QUANTUM ESPRESSO package.

of the cubic structure. Clearly, they also exhibit a gap between about 505 and 724 cm^{-1}. The softest ones at 57, 62, 63, 88, and 92 cm^{-1} correspond to mixed modes involving ReO_6 rotations and TA modes of the $Pm3m$ structure and are rather sensitive to pressure as expected [see Fig. 6(a)]. We notice a sudden change in the frequency at 2.2 GPa which may be attributed to the phase transition from the cubic $Pm3m$ to the $Im3$ phase. The rate of change in frequencies (cm^{-1}/GPa) is marked in Fig. 6(a). Clearly, the theoretical estimates of the rate of change in phonon frequency with pressure [marked in Fig. 6(a)], although very high, are somewhat smaller than the observed values (76 and 22 cm^{-1}/GPa), thereby highlighting the role of thermal fluctuations and anharmonic effects. Nevertheless, our analysis brings out the phonons in the parent high-symmetry $Pm3m$ structure of ReO_3 that are relevant to the structural transitions. From visualization of the eigenvectors of these modes of the $Im3$ phase, we find that they involve octahedral rotations at high as well as at low pressures [see Figs. 6(b) and 6(c)]. At $P \sim 2.2$ GPa, there is a striking change in the slope of the pressure dependence of frequencies of these modes, consistent with our experimental observations. The point of drastic change in the slope of ω as a function of pressure gives a rough estimate of transition pressure of the first phase transition. To precisely locate the transition pressure, we determined the enthalpy of the $Pm3m$ and $Im3$ structures. From the energy as a function of volume [Fig. 7(a)] of the $Pm3m$ and $Im3$ phases of ReO_3, it is clear that the $Im3$ phase becomes energetically more favorable as the volume decreases. Using the fit obtained with the Murnaghan equation of state to the energy versus volume curves, we determined the enthalpy as a function of volume. Our estimate of the transition pressure (the point at which the enthalpies of the two phases are equal [Fig. 7(b)]) for the $Pm3m$ to the $Im3$ phase transition is 0.1 GPa, which is smaller than the experimental value of 0.6 GPa. Errors of such magnitude are typical of DFT calculations due to its under estimation of bond lengths or lattice constants. We carried out all-electron full potential linearized augmented plane-wave calculations using WIEN2K to eliminate the errors in the structure and bond lengths arising from the use of pseudopotentials. Our estimate of the transition pressure from the enthalpy versus pressure curve (Fig. 8) obtained using WIEN2K is 0.5 ± 0.1 GPa, quite close to the experiment.

Our finding that this pressure is clearly lower than the one at which M_3 modes become unstable shows that: (a) the M_3 modes are not the *only* modes relevant to this transition and (b) that their anharmonic coupling with the TA and LA modes is important. Finally, we comment on the nature of the $Pm3m$ to $Im3$ phase transition. From our analysis of phonons, we note that the transition from the $Pm3m$ to the $Im3$ structure is driven by the instability of M_3 phonons. As seen in Fig. 5,

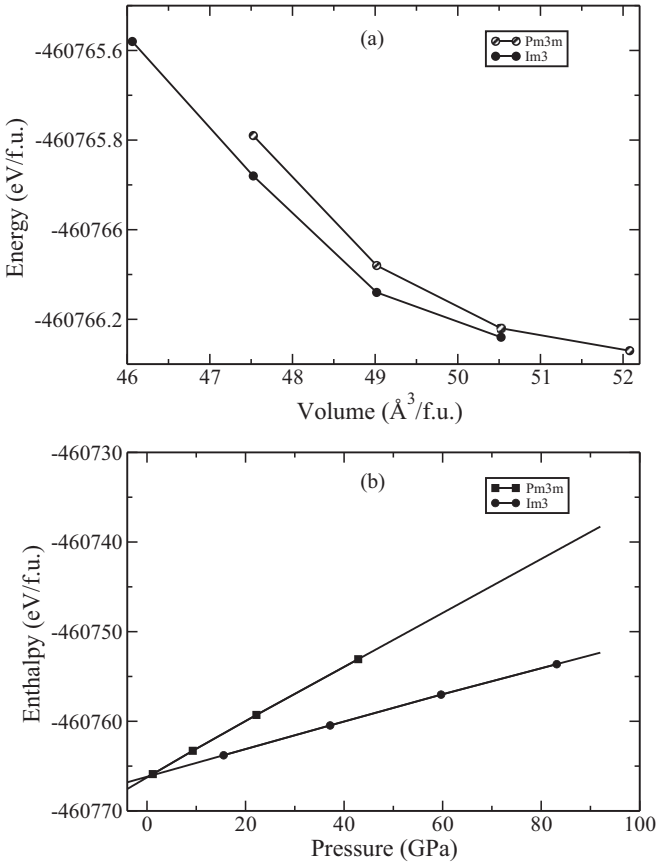

FIG. 8. (a) Total energy curve of the $Pm3m$ and the $Im3$ phases of ReO_3 and (b) their enthalpy change with pressure, obtained from all-electron calculations carried out with WIEN2K.

M_3 phonons become unstable for $P > 3$ GPa. However, based on the analysis of enthalpy of these structures as a function of P, we find that the transition occurs at a much lower pressure of $P = 0.5$ GPa. This is depicted in the sketch (see Fig. 9) of the frequency of the M phonon with pressure near the transition. We note that: (a) there is a discontinuous change in the slope of $\omega_M^2(P)$ at the transition pressure, and (b) the phonon frequency does not drop to zero at the transition. Based on this, we conclude that the transition is weakly first order as the frequency of the relevant phonon M_3 is quite low (64 cm^{-1})

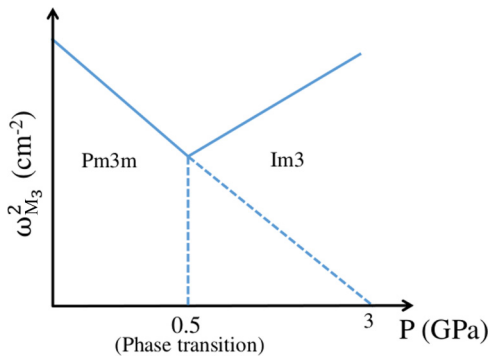

FIG. 9. (Color online) Sketch of pressure dependence of frequency of the M phonon near the phase transition.

just below the transition pressure. Although we cannot rule out an intermediate tetragonal phase, our analysis supports that it is a weakly first-order transition, driven by the third-order couplings between M_3 and acoustic modes as evident in Fig. 5. We further note that our calculations bring out clearly that phonon dispersion of the cubic $Pm3m$ phase exhibits no unstable modes at pressures above the transition pressure. Thus, the $Pm3m$ phase remains metastable even above the transition pressure and can coexist with the $Im3$ phase, which means the transition is of first order.

4. *Electron-phonon coupling*

To assess the role of electron-phonon coupling to understand the underestimation of frequencies of the IR-active modes, we estimated the electron-phonon coupling for modes at the high-symmetry wave vectors using DFT linear-response calculations. We find that modes Γ_{25}, X_5, and M_3 exhibit notable electron-phonon couplings of $\lambda = 0.016, 0.06$, and 0.01, respectively. All the modes at the R point have vanishingly small λ. This can be understood from the nature of the Fermi surface [11], which exhibits nesting with wave vectors at only X and M points. It is interesting to note that: (a) phonons M_3 and R_{25} relevant to structural transitions exhibit negligible coupling with electrons, (b) the highest-frequency modes do not couple strongly with electrons, so the dynamical corrections to their adiabatic frequencies would be small and would not explain the discrepancy between theory and experiment, and (c) only the modes that involve bond bending along the Re-O-Re chains (deviation of the Re-O-Re angle from 180°) couple strongly with electrons.

5. *Why* ReO_3 *does not exhibit transitions as a function of temperature*

As evident in its phonon dispersion [Fig. 3], ReO_3 in the cubic structure does *not* exhibit any structural instabilities at ambient pressure and 0 K. Its pressure-dependent transition involves unstable modes corresponding to rotations of ReO_6 octahedra. These modes harden with an increase in volume [see Fig. 5]. Although ReO_3 exhibits negative thermal expansion at low temperatures, this is not strong enough to make the M_3 mode unstable. As a result, the cubic structure remains stable at elevated temperatures at ambient pressure. We note that its negative thermal expansion involves the anharmonic coupling [12] that is similar to what causes the low-pressure phase transition to be weakly first order.

IV. CONCLUSIONS

In conclusion, pressure-dependent Raman measurements have been carried out on a single crystal of ReO_3 up to high pressures of 26.9 GPa at room temperature. The pressure dependence of phonon frequencies shows three phase transitions around 0.6, 3, and 12.5 GPa. The pressure dependence of the two low-frequency modes is anomalously high above 0.6 GPa, and $d\omega/dP$ changes drastically at 3 GPa. These modes further split into doublets around 12.5 GPa. We observe that the sample recovers to the initial phase upon releasing the pressure, establishing the reversibility of the transitions. From our theoretical analysis, we note that the softening

and anharmonicity of the M_3 phonon mode are relevant to the low-pressure phase transitions in ReO_3. Our estimate of the transition pressure for the low-pressure transition from the $Pm3m$ to the $Im3$ structure is 0.1 GPa, lower than the pressure at which M_3 modes become unstable. Thus, the transition has a weakly first-order character and arises from third-order anharmonic coupling between M_3 and acoustic modes.

ACKNOWLEDGMENTS

A.K.S. thanks the Department of Science and Technology (DST), Government of India for financial assistance. U.V.W. acknowledges support from a JC Bose National Fellowship of the DST. This work was performed when P. Teredesai and S. Saha were at IISc, Bangalore.

[1] C. N. R Rao and B. Raveau, *Transition Metal Oxides: Structure, Properties and Synthesis of Ceramic Oxides* (Wiley-VCH, New York/Weinheim, 1998).
[2] P. Ghosez, E. Cockayne, U. V. Waghmare, and K. M. Rabe, Phys. Rev. B, **60**, 836 (1999).
[3] J. E. Schirber and B. Morosin, Phys. Rev. Lett. **42**, 1485 (1979).
[4] J. E. Jorgensen, J. D. Jorgensen, B. Batlogg, J. P. Remeika, and J. D. Axe, Phys. Rev. B **33**, 4793 (1986).
[5] T. Chatterji and G. J. McIntyre, Solid State Commun. **139**, 12 (2006).
[6] J. E. Jorgensen, J. Staun Olsen, and L. Gerward, J. Appl. Crystallogr. **33**, 279 (2000).
[7] E. Suzuki, Y. Kobayashi, S. Endo, and T. Kikegawa, J. Phys.: Condens. Matter **14**, 10589 (2002).
[8] K. Biswas, D. V. S. Muthu, A. K. Sood, M. B. Kruger, B. Chen, and C. N. R. Rao, J. Phys.: Condens. Matter **19**, 436214 (2007).
[9] J. Purans, A. Kuzmin, E. Cazzanelli, and G. Mariotto, J. Phys.: Condens. Matter **19**, 226206 (2007).
[10] P. B. Allen and W. W. Schulz, Phys. Rev. B **47**, 14434 (1993).
[11] M. G. Stachiotti, F. Corà, C. R. A. Catlow, and C. O. Rodriguez, Phys. Rev. B **55**, 7508, (1997).
[12] U. D. Wdowik, K. Parlinski, T. Chatterji, S. Rols, and H. Schober, Phys. Rev. B **82**, 104301 (2010).
[13] A. Ferretti, D. B. Rogers, and J. B. Goodenough, J. Phys. Chem. Solids **26**, 2007 (1965).
[14] H. K. Mao, P. M. Bell, J. W. Shaner, and D. J. Steinberg, J. Appl. Phys. **49**, 3276 (1978).
[15] P. Giannozzi, S. Baroni, N. Bonini, M. Calandra, R. Car, C. Cavazzoni, D. Ceresoli, G. L. Chiarotti, M. Cococcioni, I. Dabo, A. D. Corso, S. de Gironcoli, S. Fabris, G. Fratesi, R. Gebauer, U. Gerstmann, C. Gougoussis, A. Kokalj, M. Lazzeri, L. Martin-Samos, N. Marzari, F. Mauri, R. Mazzarello, S. Paolini, A. Pasquarello, L. Paulatto, C. Sbraccia, S. Scandolo, G. Sclauzero, A. P. Seitsonen, A. Smogunov, P. Umari, and R. M. Wentzcovitch, J. Phys.: Condens. Matter **21**, 395502 (2009).
[16] D. Vanderbilt, Phys. Rev. B **41**, 7892 (1990).
[17] A. M. Rappe, K. M. Rabe, E. Kaxiras, and J. D. Joannopoulos, Phys. Rev. B **41**, 1227 (1990).
[18] P. Blaha, K. Schwarz, G. Madsen, D. Kvasnicka, and J. Luitz, *WIEN2k, An Augmented Plane Wave + Local Orbitals Program for Calculating Crystal Properties* (Karlheinz Schwarz, Techn. Universität Wien, Austria, 2001).
[19] A. Togo, F. Oba, and I. Tanaka, Phys. Rev. B **78**, 134106 (2008).
[20] M. Ishii, T. Tanaka, T. Akahane, and N. Tsuda, J. Phys. Soc. Jpn. **41**, 908 (1976).
[21] U. V. Waghmare and K. M. Rabe, Phys. Rev. B **55**, 6161 (1997).